Journal of Hydroscience and Hydraulic Engineering
Vol. 24, No.1 May, 2006, 23-40

SHORT PERIODIC VELOCITY COMPPNENTS IN THE TONE RIVER ESTUARY

By

K. Shimizu

Tokyo Institute of Technology, Tokyo Japan
Present: Centre for Water Research, University of Western Australia, Perth, Australia

and

T. Ishikawa

Tokyo Institute of Technology, Tokyo Japan

SYNOPSIS

Velocity and water level fluctuations over a the period of 30 to 60 minutes observed in the Tone River Estuary is analyzed to investigate the vertical structure of velocity field, the frequency characteristics, and the force exciting the fluctuation. An examination of field data shows that the fluctuation is barotropic and forced by offshore water level fluctuation. A spectrum analysis indicates that the fluctuation is due to two mechanisms: resonance at natural periods and oscillation forced by a dominant offshore fluctuation. This finding is confirmed by a comparison of frequency response functions estimated from observations and the theory of radiation and friction damping, which shows good agreement for $T > 0.5$ hr. The theoretical solution also shows that friction is a dominant mechanism of damping at low frequency. Fluctuation appears to increase the peak value of the bottom shear stress and the resuspension rate of sediment in the estuary significantly.

INTRODUCTION

Sediment dynamics in estuaries are characterized by diurnal or semi-diurnal change of suspended sediment concentration, which is caused by mechanisms such as tidal asymmetry (Allen *et al.* (1)), internal tidal asymmetry (Jay and Musiak (2)), and estuarine circulation (Postma (3)).

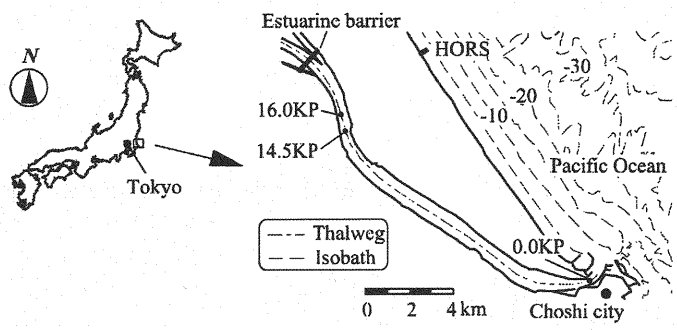

Fig. 1 Location and plane view of the Tone River Estuary.

However, (the) observations on sediment dynamics in the Tone River Estuary (Shimizu *et al.* (4), (5)) indicate that the resuspension of the sediment is strongly influenced by velocity fluctuation over the period of 30 to 60 minutes (hereafter we call it "short-period fluctuation" in the sense that the period is shorter than that of tide). Therefore, the aim of this study is to investigate the vertical structure, the frequency characteristics, the exciting force, and the factors determining the response of the estuary based on observational and theoretical analysis.

STUDY SITE

The Tone River Estuary is a shallow weakly mixed salt-wedge estuary located in southeast part of Japan (Fig. 1). The channel is almost straight with a length of 20 km and a depth of about 4 m. The Tone River Estuarine Barrier lies at the upper limit of the estuary, which controls freshwater discharge and saline water intrusion into the inland to enhance water intake and to prevent salt damage upstream of the barrier. Under normal discharge conditions, the head of salt-wedge is steadily located right below the estuarine barrier (Ishikawa *et al.* (6)).

VERTICAL STRUCTURE

First, the vertical structure of the short-period fluctuation of velocity field is examined using the field data obtained on 20th of April 2003. During this field observation, an Acoustic Doppler Current Profiler (ADCP, Aquadopp; Nortek AS) and an Acoustic Doppler Velocimeter (ADV, Vector; Nortek AS) were deployed on the bottom at 16.0 KP (*see* Fig. 1) to measure vertical velocity profile and turbulence at 0.15 m above the bottom over a tidal cycle. Turbulent flux of suspended sediment (SS) was calculated using suspended sediment concentration estimated from acoustic intensity data. The details of the observation and the technique used are reported by Shimizu *et al.* (4), (5).

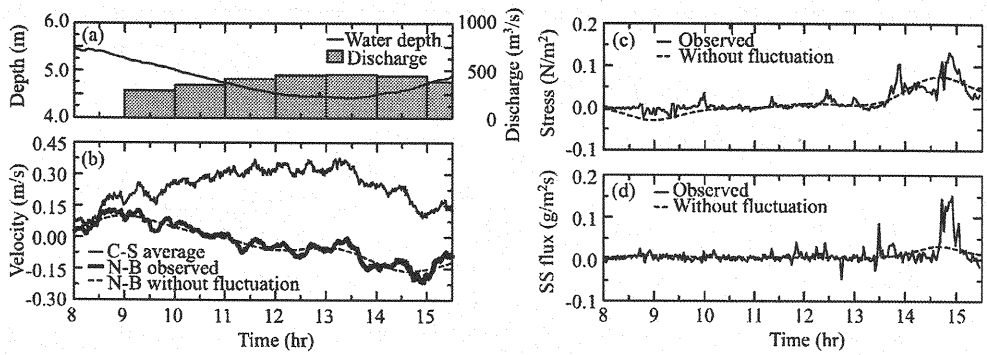

Fig. 2 Results of the field observation on 20th of April, 2003 at 16.0 KP. (a) water level and discharge from the Tone River Estuarine Barrier, (b) cross-sectional average velocity (C-S average; thin line) and near-bottom velocity (N-B observed; bold line), (c) Near-bottom Reynolds stress, and (d) vertical SS flux. The dashes in (b), (c), and (d) show near-bottom average velocity, the Reynolds stress, and SS flux without a short-period fluctuation, respectively.

Fig. 2 shows major results of this observation: Panel (a) shows water depth at 16.0 KP (solid line) and discharge from the estuarine barrier (vertical bar); Panel (b) shows the cross-sectional average velocity calculated from velocity profile measured by the ADCP (thin solid line) and a two-minute-averaged near-bottom velocity measured by the ADV (bold solid line, both positive in downstream direction); Panel (c), (d) show the Reynolds stress (positive when the water column receive force in upstream direction) and turbulent SS flux (positive in upward direction), respectively. The significance of the dashes in the figure will be explained in a later section.

The trend of cross-sectional average velocity (thin line in Fig. 2 (b)) and near-bottom velocity (bold line in Fig. 2 (b)) do not match in the timescale of tide because the latter is measured in the salt-wedge. However, the amplitude and phase of fluctuation over the period of 30 to 60 min match well. This fact indicates that the short-period velocity fluctuation is barotropic. Reynolds stress (Fig. 2 (c)) and SS flux (Fig. 2 (d)) also show considerable fluctuation corresponding to the velocity fluctuation. This effect will be discussed in the section entitled "DISCUSSION".

FREQUENCY CHARACTERISTICS

In order to investigate the frequency characteristics of the short-period fluctuation in detail, data set obtained in a monitoring observation conducted from 1st to 10th of August 2001 is used here. During the period of observation, the vertical velocity profile and water level at 14.5 KP (*see* Fig. 1) were measured by an ADCP (Aquadopp; Nortek AS) placed on the bottom. Two-minute-averaged velocity and water level were recorded every five minutes. The offshore water level was measured at the Hazaki Oceanographical Research Station (HORS), which is a research facility with a

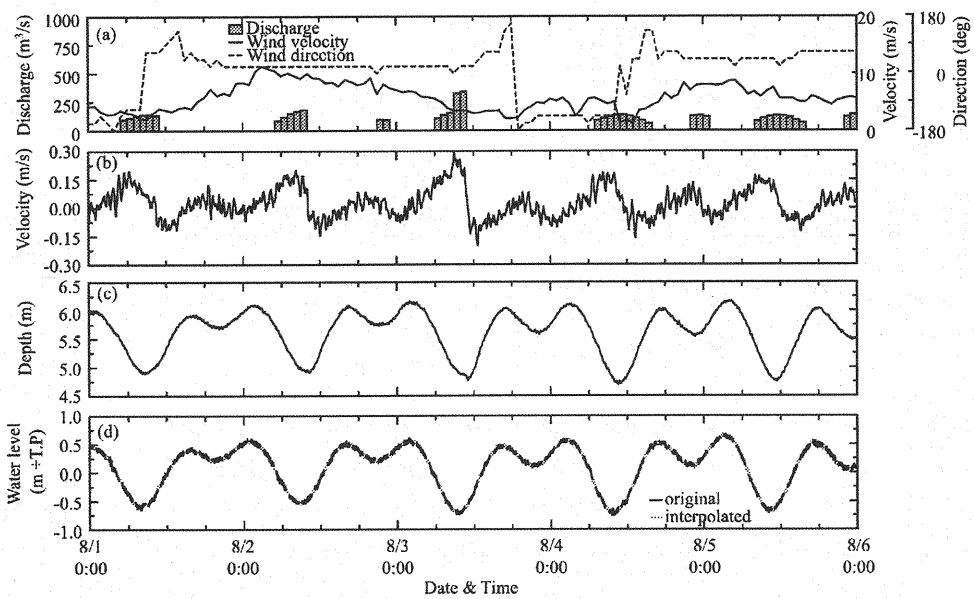

Fig. 3 Results of the monitoring observation from 1st to 5th of August, 2001. (a) discharge from the estuarine barrier, and the wind velocity and the wind direction at Choshi, (b) the cross-sectional average velocity in longitudinal direction at 14.5 KP (positive in downstream), (c) water level at 14.5 KP, and (d) observed water level at the HORS (solid line, low-pass filtered) and interpolated water level by AR model (dotted line).

427m-long pier located near the Tone River Estuary (*see* Fig. 1). The water level was measured for 94 minutes with the frequency of 2 Hz from every odd hours by means of an aerial-emission-type ultrasonic wave gage located about 400 m offshore from the shore line, where water depth is about 5 m.

Fig. 3 shows the results of the first half of the monitoring observation. Fig. 3 (a) shows discharge from the estuarine barrier (vertical bar), and hourly wind velocity (solid line) and wind direction (dashes) at Choshi city (*see* Fig. 1). The cross-sectional average velocity (positive in the downstream direction) and water level at 14.5 KP are shown in Fig. 3 (b), (c), respectively. Fig. 2 (d) shows the water level at the HORS with a solid line for the observed water level and dotted line for the interpolated (the method used for interpolation will be explained later in this section.) A low-pass filter with the cutoff frequency of 1/2 min^{-1} is applied to the observed water level in order to eliminate water level fluctuation due to wind waves and swells.

The cross-sectional average velocity (Fig. 3 (b)) shows significant and almost steady velocity fluctuation with the period of 30 to 60 min. Although amplitude is small, fluctuation with similar frequency is also observed in water level (Fig. 2 (c)). The reason for this is that the fluctuation is barotropic as shown in the previous section. Data in the second half of the monitoring observation

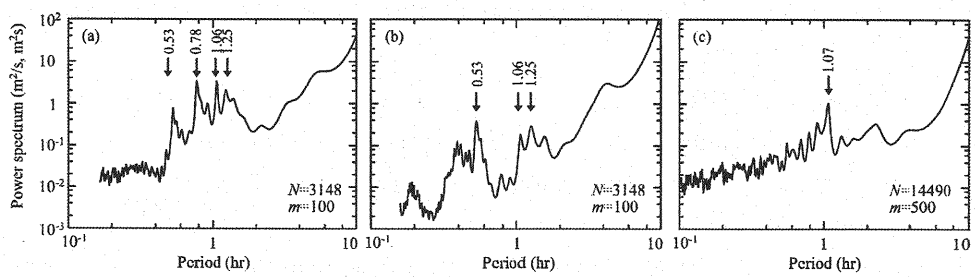

Fig. 4 Power spectra. (a) cross-sectional average velocity at 14.5 KP, (b) water level at 14.5 KP, and (c) water level at the HORS. N is the total number of data and m is lag number used for spectrum estimation. Numbers next to arrows represent the period at the peak in hr.

shows similar characteristics.

In order to investigate the frequency characteristics, power spectra of cross-sectional average velocity and water level are estimated by the Burg method (e.g. Hino (7), Wu (8)). Lag number m used in the method is chosen in the way to minimize Final Prediction Error (FPE) of both velocity and water simultaneously. The estimated power spectra of velocity and water level are shown in Fig. 4 (a), (b), respectively (Fig. 4 (c) shows the power spectrum of water level at the HORS, which will be explained in the next section). The spectra show several distinct peaks as indicated by arrows in the figure. The periods at the peaks are 1.25, 1.06, 0.78, and 0.53 hr, though the spectrum of water level (Fig. 4 (b)) lacks the peak at 0.78 hr. This is because 14.5 KP is located at the node of third mode as shown in Fig. 8 (explained in "*comparison with field data*"). The spectrum of velocity with period shorter than 0.5 hr is flat at a low level which is probably due to noise.

Assuming that the estuary is one-dimensional straight channel, the periods of seiche in the Tone River Estuary (or natural period of the estuary) are given approximately by:

$$T_n = \frac{4L}{(2n-1)\sqrt{gh}}, \quad n = 1, 2, 3\cdots \tag{1}$$

where T_n = periods of seiche of mode n; L = the length of an estuary; g = acceleration due to gravity; h = mean water depth (cross-sectional area divided by the width of water surface); and n = order of the mode. Given that the length of the Tone River Estuary is about 20 km and the mean water depth at mean sea level is 3.9 m, the period of the fundamental mode is 3.59 hr, and those of the higher harmonics are 1.20, 0.72, 0.51 hr for n = 2, 3, 4, respectively. These periods coincide with the periods of peaks in the spectra, indicating that these fluctuations are caused by longitudinal seiche. However, there is no natural period which corresponds to the period of 1.06 hr. The fluctuation is not due to a seiche but the oscillation forced by dominant offshore water level fluctuation as shown in the next section.

EXCITING FORCE

Oscillation in estuaries, harbors, and bays may be caused by exciting forces, such as waves incoming from offshore, freshwater discharge, wind-induced surface shear, and atmospheric pressure disturbance (e.g. Horikawa (9)). Here, the force exciting the short-period fluctuation is investigated by examining these possible factors.

As shown in Fig. 3 (a), the estuarine barrier discharges freshwater only during low water. The sudden change of discharge when the gates are opened or closed may excite oscillation. However, a short-period velocity fluctuation is almost steady and does not correspond to the change of the discharge (Fig. 3 (a), (b)), indicating that discharge is not the primary exciting force. Wind velocity and atmospheric pressure varied from 1 m/s to more than 10 m/s (Fig. 3 (a)) and from 1010 to 1020 hPa (not shown), respectively, during the observation with the timescale of a half to few days. Again, these changes do not correspond to the almost steady short-period velocity fluctuation. On the other hand, Hayashi *et al.* (10) observed roughly steady wave over the period of 60 to 100 min outside of the port of Kashima, which is located about 25 km north of the Tone River. They concluded that the wave is shelf seiche. Because the period is close to that of the short-period fluctuation, such wave may excite the short-period fluctuation. Therefore, frequency characteristic of waves incoming from the offshore is examined.

The power spectrum of the water level at the HORS is estimated as follows. Before estimating the spectrum, interpolation of water level data is necessary because gaps of 26 min length every 2 hours make it difficult to estimate power spectrum in the period range of 30 to 60 min. The AR model is chosen to fill the gaps. The coefficients are calculated by applying the Burg method to all available segments (de Waele and Broersen (11)). Interpolated data is denoted by the dotted line in Fig. 2 (d). After interpolation, the Burg method is applied to estimate the spectrum of water level at the HORS.

The power spectrum of water level at the HORS is shown in Fig. 4 (c). A distinct peak is seen at 1.07 hr, which is probably caused by shelf seiche (Hayashi *et al.* (10)). At this period, distinct peaks are also observed in the spectra of velocity and water level at 14.5 KP (Fig. 4 (a) and (b)). This finding indicates that at least part of the short-period fluctuation is caused by the offshore water level fluctuation. On the other hand, the spectrum of water level at the HORS does not have peaks at 1.20, 0.72, and 0.51 hr. Because the periods are natural periods of the estuary, these peaks may be caused by resonance. To examine this possibility, frequency response functions of velocity and water levels against offshore water level fluctuation are examined in the next section.

FREQUENCY RESPONSE FUNCTIONS

Estimation from observation

The frequency response functions of velocity and water levels in the estuary against offshore water level fluctuation are defined as:

$$|H_U(x,\omega)|^2 = \left(\frac{U(x,\omega)}{\zeta_0(\omega)}\frac{h}{c}\right)^2 = \frac{P_U(x,\omega)}{P_{\zeta 0}(\omega)}\left(\frac{h}{c}\right)^2 \tag{2}$$

$$|H_\zeta(x,\omega)|^2 = \left(\frac{\zeta(x,\omega)}{\zeta_0(\omega)}\right)^2 = \frac{P_\zeta(x,\omega)}{P_{\zeta 0}(\omega)} \tag{3}$$

where x = longitudinal distance; ω = angular frequency; H_U, H_ζ = frequency response function of velocity and water level in the estuary against offshore water level fluctuation, respectively; U = amplitude of cross-sectional average velocity; ζ, ζ_0 = amplitude of water level in the estuary and the offshore, respectively; and c = phase velocity (= $(gh)^{1/2}$). H_U is normalized by $\zeta_0 c/h$ based on analytical solution of forced oscillation in a straight channel (*see* Eq. 5).

$|H_U|^2$ and $|H_\zeta|^2$ calculated from the spectra shown in Fig. 4 are shown in Fig. 5 (The dashes shows theoretically derived frequency response function, which is explained in "theoretical analysis"). $|H_U|^2$ and $|H_\zeta|^2$ show peaks corresponding to the natural periods of the estuary (1.20, 0.72, 0.51 hr), indicating that offshore water level fluctuation is amplified by resonance ($|H_U|^2$ and $|H_\zeta|^2$ also show peaks of fundamental mode (3.59 hr), which are not clear in the power spectra shown in Fig. 4 (a), (b)). It indicates that the oscillations during these periods are caused by resonance with offshore water level fluctuation. One the other hand, the frequency response functions do not have peaks at T = 1.06 hr. This means that short-period fluctuation during this period is not caused by resonance but by the dominant offshore water level fluctuation at the period.

The above analysis of observational data qualitatively shows that the short-period fluctuation except T = 1.06 hr is caused by resonance. However, a quantitative evaluation of the frequency response functions shown in Fig. 5 is necessary. Therefore, frequency response functions will be derived theoretically and compared with those estimated from the observation.

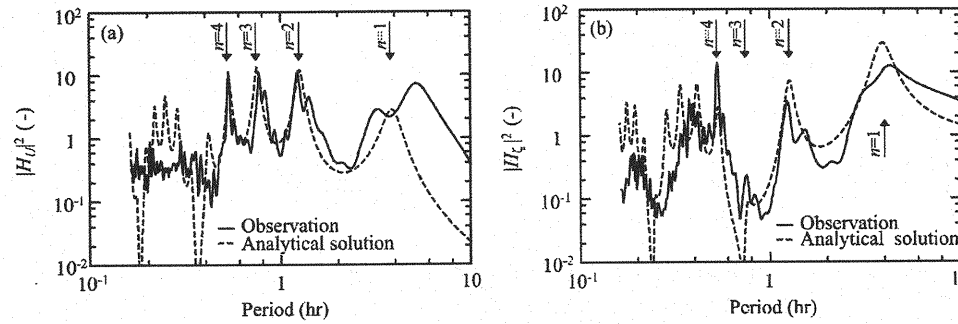

Fig. 5 Frequency response functions at 14.5KP against offshore water level fluctuation. (a) cross-sectional average velocity, (b) water level. Solid line: estimation from observation, dashes: theoretical ones calculated from Eqs. 25 and 26. The arrows and *n* next to them indicate resonant frequency and order of mode, respectively.

Analytical solution

The simplest model for the response of a long straight estuary against sinusoidal water level fluctuation at the mouth ($\zeta = \zeta_0 \cos(\omega t)$) is given by (e.g. Horikawa (9)):

$$\zeta = \zeta_0 \frac{\cos(kx')}{\cos(kL)}\cos(\omega t);\ U = \frac{\zeta_0 c}{h}\frac{\sin(kx')}{\cos(kL)}\sin(\omega t) \qquad (4)$$

where ζ = surface water displacement; U = cross-sectional average velocity; ζ_0 = surface water displacement at the mouth; k = wave number; x' = distance from the estuarine barrier (*see* Fig. 6); and t = time. Because this solution does not include any damping mechanism, amplitude becomes infinite at the resonant frequency given by Eq. 1. To derive a more realistic solution, some damping mechanism needs to be included. Several mechanisms have been considered in previous studies. Miles and Munk (12) considered that radiation of wave from a harbor to the sea is the primary damping mechanism, and Ippen and Goda (13) and Goda (14) elaborated the theory. Unluata and Mei (15) developed a theory that accounts for turbulence loss at the narrow entrance of a harbor. The bottom and sidewall friction may be important if water body is shallow or narrow (e.g. Cerovecki *et al.* (16)). Friction would be important because Tone River Estuary is shallow, narrow, and long, while turbulence loss at the mouth would be insignificant because the width of the mouth is the same as that of river channel. Therefore, in this study, a theory of Ippen and Goda (13) and Goda (14) is extended to incorporate friction damping.

An ideal geometry with a long straight estuary and the sea connected to the estuary is used for analysis (Fig. 6). As was done by Ippen and Goda (13) and Goda (14), the following assumptions are made: 1) incoming wave with constant period propagating perpendicular to the coastline; 2) perfect reflection at the coast; 3) constant water depth; 4) small amplitude compared to the water

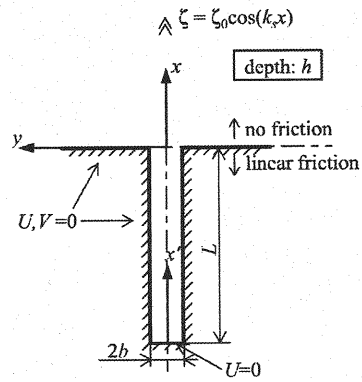

Fig. 6 Geometry and boundary conditions used for theoretical analysis.

depth. In order to include friction, linear friction in the estuary is assumed (determination of linear friction coefficient will be discussed in the following section). Friction in the sea is neglected. Based on the results of our observation, discharge from the estuarine barrier and transverse oscillation in the estuary are not matters to consider in this research.

Shallow water equations with linear friction are written as:

$$\frac{\partial \zeta}{\partial t} = -h\left(\frac{\partial U}{\partial x} + \frac{\partial V}{\partial y}\right);\ \frac{\partial U}{\partial t} = -g\frac{\partial \zeta}{\partial x} - \gamma U;\ \frac{\partial V}{\partial t} = -g\frac{\partial \zeta}{\partial y} - \gamma V \tag{5}$$

where x, y = horizontal coordinates taken as shown in Fig. 6; U, V = depth averaged velocity in x and y direction, respectively, and γ = linear friction coefficient. The above equations can be arranged to derive an equation for ζ:

$$\frac{\partial^2 \zeta}{\partial t^2} + \gamma\frac{\partial \zeta}{\partial t} - gh\left(\frac{\partial^2 \zeta}{\partial x^2} + \frac{\partial^2 \zeta}{\partial y^2}\right) = 0 \tag{6}$$

Since surface waves excited by sinusoidal forcing is considered, ζ is assumed to be periodic:

$$\zeta = f(x,y)e^{i\omega t} \tag{7}$$

Substituting Eq. 7 into Eq. 6 yields:

$$\frac{\partial^2 f}{\partial x^2} + \frac{\partial^2 f}{\partial y^2} + \frac{\omega^2 - i\gamma\omega}{gh} f = 0 \tag{8}$$

As was done by Ippen and Goda (13) and Goda (14), water level in the sea (f_s) and in the estuary (f_e) are derived separately, and later average water level and velocity at the mouth is matched to derive the complete solution. Boundary conditions are as follows. Far offshore, waves become standing waves parallel to coastline:

$$f_s(x,y) = \zeta_0 \cos(k_s x) \quad \text{as} \quad x^2 + y^2 \to \infty \tag{9}$$

At the estuarine barrier and the coast, normal velocity (gradient of water level) is zero:

$$\frac{\partial f_e}{\partial x} = 0 \quad \text{at} \quad x = -L \tag{10}$$

$$\frac{\partial f_s}{\partial x} = 0 \quad \text{at} \quad x = 0, \ |y| > b \tag{11}$$

where b = half width of the mouth. At the mouth, the average water level and velocity (gradient of water level) over the mouth is continuous:

$$\overline{\zeta_s(0,y)} = \overline{\zeta_e(0,y)} \quad \text{at} \quad x = 0, |y| < b \tag{12}$$

$$\left(\frac{\partial \overline{f_s}}{\partial x}\right)_{x=0} = \left(\frac{\partial \overline{f_e}}{\partial x}\right)_{x=0} = k_s a e^{i\varphi} \quad \text{at} \quad x = 0, |y| < b \tag{13}$$

where k_s = wave number in the sea (= ω / c); and a, φ = constant representing velocity and phase shift at the mouth, respectively. Over bar denotes the average over the width of the mouth.

In the sea, f_s is separated into standing waves that satisfies Eq. 9 and disturbance radiated from the river mouth f_r:

$$f_s(x,y) = \zeta_0 \cos(k_s x) + f_r(x,y) \tag{14}$$

This simplifies offshore boundary condition (Eq. 9) as:

$$f_r(x,y) = 0 \quad \text{as} \quad x^2 + y^2 \to \infty \tag{15}$$

After applying the Fourier transform to Eq. 8, a general solution is derived:

$$F_r(x,y) = C_1(k_{sy}) e^{\sqrt{k_{sy}^2 - k_s^2}\, x} + C_2(k_{sy}) e^{-\sqrt{k_{sy}^2 - k_s^2}\, x} \tag{16}$$

where F_r = Fourier transform of f_r; k_{sy} = wave number in y direction; and C_1, C_2 = constants of integration. When $k_{sy} > k_s$, C_1 must be 0 to satisfy Eq. 15, while when $k_{sy} < k_s$, again C_1 must be 0 because the first term represents incoming wave but f_r is assumed to be wave radiating from the estuary (Ippen and Goda (13), Goda (14)). By applying boundary conditions at the mouth (Eq. 11), C_2 can be determined, and averaging over the river mouth yield:

$$\overline{f_r(0,y)} = \frac{1}{2b} \int_{-b}^{b} f_r(0,y) dy = a e^{i\varphi} \left[i\psi_1 - \psi_2 \right] \tag{17}$$

where

$$\psi_1(k_s b) = \frac{2}{\pi} \int_0^{k_s b} \frac{k_s b \sin^2(\alpha)}{\alpha^2 \sqrt{(k_s b)^2 - \alpha^2}} d\alpha; \quad \psi_2(k_s b) = \frac{2}{\pi} \int_{k_s b}^{\infty} \frac{k_s b \sin^2(\alpha)}{\alpha^2 \sqrt{\alpha^2 - (k_s b)^2}} d\alpha \tag{18}$$

are radiation functions (Ippen and Goda (13)), which is shown in Fig. 7.

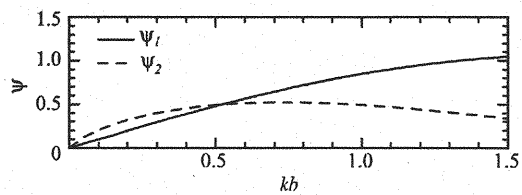

Fig. 7 Radiation functions ψ_1 and ψ_2 defined by Eq. 18.

In the estuary, the general solution of Eq. 8 is an exponential function with the wave number k_e. Since friction is taken into account, k_e becomes complex whose real part k_{er} and imaginary part k_{ei} are given by:

$$k_e = k_{er} - ik_{ei};\ k_{er} = \frac{\omega}{\sqrt{gh}}\sqrt{\frac{1+\sqrt{1+(\gamma/\omega)^2}}{2}};\ k_{ei} = \frac{\gamma}{2\sqrt{gh}}\sqrt{\frac{2}{1+\sqrt{1+(\gamma/\omega)^2}}} \quad (19)$$

f_e is determined by applying Eqs. 10 and 13. Substituting f_e into Eqs. 7 and 9 yield

$$\zeta(x,t) = -ia\frac{k_s}{k_e}\frac{\cosh(ik_e x')}{\sinh(ik_e L)}e^{i(\omega t+\varphi)};\ U(x,t) = ia\frac{ck_s}{k_e}\frac{\sinh(ik_e x')}{\sinh(ik_e L)}e^{i(\omega t+\varphi)} \quad (20)$$

here $x' = L + x$ is introduced for convenience.

At the mouth, the solution in the sea (Eq. 17) and the solution in the estuary (Eq. 20) are matched to satisfy Eq. 12.

$$\zeta_0 e^{i\omega t} + a(i\psi_1 - \psi_2)e^{i(\omega t+\varphi)} = -ia\frac{k_s}{k_e}\frac{\cosh(ik_e x')}{\sinh(ik_e L)}e^{i(\omega t+\varphi)} \quad (21)$$

Since this equation is identical to the equation of complex valuable, a and φ can be determined as follows:

$$a = \frac{\zeta_0}{\sqrt{(S_1+\psi_1)^2 + (-S_2+\psi_2)^2}};\ \tan(-\varphi) = \left(\frac{S_1+\psi_1}{-S_2+\psi_2}\right) \quad (22)$$

where

$$S_1 = \frac{k_s}{k_{er}^2 + k_{ei}^2}\frac{k_{er}\sinh(2k_{ei}L) - k_{ei}\sin(2k_{er}L)}{\cosh(2k_{ei}L) - \cos(2k_{er}L)} \quad (23)$$

$$S_2 = \frac{k_s}{k_{er}^2 + k_{ei}^2}\frac{k_{er}\sin(2k_{er}L) - k_{ei}\sinh(2k_{ei}L)}{\cosh(2k_{ei}L) - \cos(2k_{er}L)} \quad (24)$$

Note that the sign in Eq. 22 is kept to avoid ambiguity of φ by π. The solutions of velocity and the water level in the estuary are given by Eqs. 19, 20, 22, 23, and 24. If the effect of radiation and friction is neglected ($k_s = k_{er}$, $k_{ei} = \psi_1 = \psi_2 = 0$), the solutions are reduced to Eq. 4 (note that $a = \zeta_0 |\sin(k_{er}L)|/|\cos(k_{er}L)|$ and $\varphi = \pi$ or 0 so that always $ae^{i\varphi} = -\zeta_0 \sin(k_{er}L)/\cos(k_{er}L)$). Taking square of the solutions followed by normalization yields frequency response functions for water levels and velocity

$$\left|H_{\zeta}(x',\omega)\right|^2 = \frac{1}{(S_1+\psi_1)^2+(S_2-\psi_2)^2}\left(\frac{k_s}{|k_e|}\right)^2 \frac{\cosh(2k_{ei}x')+\cos(k_{er}x')}{\cosh(2k_{ei}L)-\cos(k_{er}L)} \tag{25}$$

$$\left|H_{U}(x',\omega)\right|^2 = \frac{1}{(S_1+\psi_1)^2+(S_2-\psi_2)^2}\left(\frac{k_s}{|k_e|}\right)^2 \frac{\cosh(2k_{ei}x')-\cos(k_{er}x')}{\cosh(2k_{ei}L)-\cos(k_{er}L)} \tag{26}$$

If friction is overlooked ($k_s = k_{er}$, $k_{ei} = 0$), Eq. 25 is reduced to the solution given by Ippen and Goda (13) and Goda (14).

Equivalent linear friction coefficient

The analytical solution derived above assumes linear friction for simplicity. However, frictional force at bottom is proportional to square of velocity. Thus, linear friction coefficient must be determined in the way that the prediction by the theory with linear friction is consistent with that with quadratic friction. One way to achieve this is the use of "equivalent" linear friction coefficient, which is derived by equating total energy dissipated over one period by linear friction to that by quadratic friction. The method is based on the fact that, in steady state, the energy input by external force must be dissipated to keep the total energy constant, regardless of dissipation mechanism (Timoshenko *et al.* (17), Ono (18)).

In order to calculate equivalent linear friction coefficient, spatial distribution of velocity is necessary. To derive simple expression for equivalent linear friction coefficient, velocity field given by Eq. 20 is simplified as follows. As a first approximation, it is possible to assume that friction is small so that $\cosh(k_iL) \approx 1$, $\sinh(k_iL) \approx k_iL$ (in fact, $k_{ei}L = 0.154$ using the linear friction coefficient given below). In addition, because friction is important only near resonance frequencies (Timoshenko *et al.* (17), Ono (18), also *see* Fig. 9) and only when friction dominates dissipation, it is assumed that $\cos(k_{er}L) \approx 0$ and $\sin(k_{er}L) \approx (-1)^{n-1}$ (near resonant frequency), and $\psi_1, \psi_2 << k_iL$ (friction damping dominates). These assumptions simplify velocity field as:

$$U(x',t) = \frac{(-1)^n}{k_{ei}L}\frac{c\zeta_0}{h}\sin(k_{er}x')\sin(\omega t+\varphi) \tag{27}$$

Using this simplified velocity field, dissipated energies over a period by linear friction ε_{lin} and by quadratic friction ε_{quad} can be calculated as follows:

$$\varepsilon_{lin} = 2b\int_0^L\left(\oint(\gamma U)d\xi\right)dx = 2b\int_0^L\int_0^T \gamma U^2 dtdx = \frac{bLT}{2}\gamma\left(\frac{c\zeta_0}{hk_{ei}L}\right)^2 \tag{28}$$

$$\varepsilon_{quad} = 2b\int_0^L\left(\oint\left(\frac{f_b}{2h}|U|U\right)d\xi\right)dx = \frac{bf_b}{R}\int_0^L\int_0^T |U|U^2 dtdx = \frac{16bf_bLT}{9\pi^2R}\left(\frac{c\zeta_0}{hk_{ei}L}\right)^3 \tag{29}$$

where ξ = horizontal displacement; R = hydraulic radius. $\oint$ represents integral over one period.

Table 1 Values used to calculate frequency response function and mode shape.

ζ_0	0.02	(m)	R	3.9	(m)
L	20000	(m)	n	0.02	($s/m^{1/3}$)
b	375	(m)	f_b	0.0050	(-)
h	3.9	(m)	γ	9.5×10^{-5}	(s^{-1})

Equating these dissipated energy and using the relationship $k_{ei} = \gamma/2c$ (from Eq. 19) gives an expression for equivalent linear friction coefficient

$$\gamma = \frac{8c}{3\pi}\sqrt{\frac{f_b\zeta_0}{hRL}} \tag{30}$$

To calculate the value, root mean square of low-pass filtered water level fluctuation at the HORS is used as ζ_0. A quadratic friction coefficient f_b is calculated from the following relation (e.g. Ikeda (19)).

$$f_b = \frac{2gn_{Manning}^{\ 2}}{R^{1/3}} \tag{31}$$

where $n_{Manning}$ = Manning's roughness coefficient. Common value of $n_{Manning}$ for lower reaches of the Tone River ($n_{Manning} = 0.02\ s\cdot m^{-1/3}$) and R calculated from bathymetry data at mean sea level ($R = 3.9$ m) gives $f_b = 0.0050$. Substituting these values into Eq. 30 gives $\gamma = 9.5\ \times10^{-5}\ s^{-1}$.

Comparison of observational and analytical frequency response functions

Using the equivalent liner friction coefficient calculated above, frequency response functions of velocity and water level calculated from Eqs. 25 and 26 are presented in Fig.4 by dashes. The parameters used in the calculation are summarized in Table 1. The periods and the height of the peaks at resonant periods for $n = 1$ to 4 agree very well. For frequencies higher than 0.5 hr^{-1}, the agreement is poor. This is probably because sampling frequency (1/5 min^{-1}) is too low and an error in the position of measurement (x') becomes significant for this frequency range. Longitudinal distribution of $|H_U|$ and $|H_\zeta|$ (equivalent to normalized amplitude) for $n = 1$ to 4 are shown in Fig. 8. From $|H_\zeta|$ (Fig. 8 (b)), it is clear that 14.5 KP is located at the node of third mode. This explains why the spectrum of water level lacks peak at $n = 3$ in Fig. 4 (b). These findings confirm that short-period fluctuation is caused by resonance between the estuary and offshore water level fluctuation.

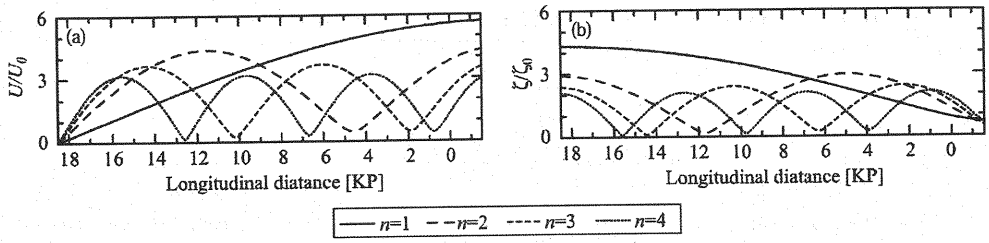

Fig. 8 Absolute value of normalized frequency response functions (equivalent to amplitude of mode shape). (a) velocity and (b) water level calculated by Eqs. 25 and 26. KP represents the distance from the river mouth of the Tone River.

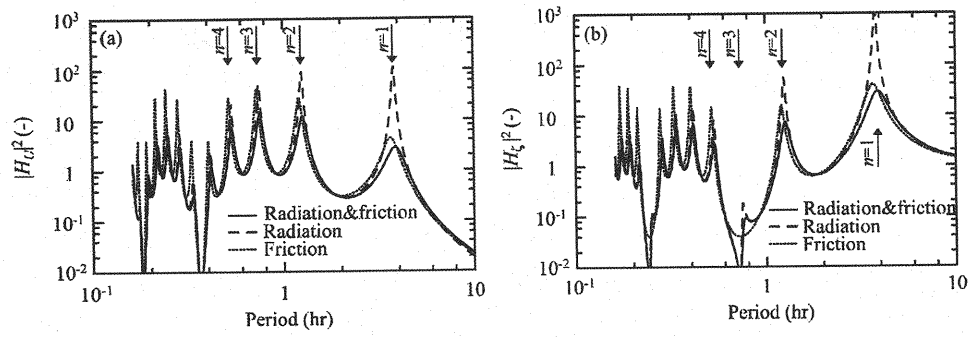

Fig. 9 Frequency response functions of velocity (a) and water level (b). Solid, dashed and dotted lines show frequency response function with both radiation and friction damping, with radiation damping, and with friction damping, respectively.

DISCUSSION

In order to examine the influence of radiation and friction damping, analytical solutions only with radiation damping and those only with friction damping are calculated and compared to those with both damping mechanisms. Fig. 9 shows the comparison. The figure illustrates a dominance of friction damping at lower frequency (n = 1), and similar contribution of radiation and friction damping at higher frequency (n = 3, 4). Unlike the case of harbors, bottom friction is important as a damping mechanism because the Tone River Estuary is long (note that γL is proportional to $L^{1/2}$).

Lasting, it is necessary to estimate the influence of short-period fluctuation on bottom stress and resuspension of sediment. For this purpose, time series of Reynolds stress and SS flux without the influence of short-period fluctuation are estimated as follows. First, correlations between near-bottom mean velocity and Reynolds stress, and Reynolds stress and turbulent SS flux are obtained. These correlations are shown in Fig. 9 (two data points enclosed by dashed circle in panel (b) are excluded to obtain regression line because the trend is different from the others).

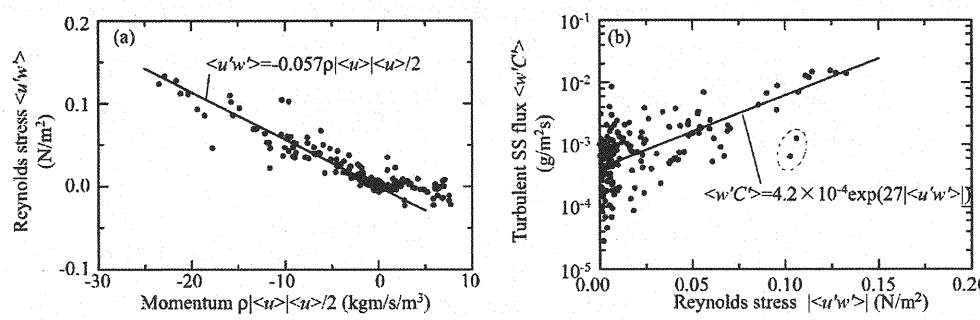

Fig. 10 Correlations among near-bottom velocity, Reynolds stress, and SS flux measured on 20/Apr/2005. (a) velocity and Reynolds stress, (b) Reynolds stress and SS flux.

Then, near-bottom mean velocity shown by the bold line in Fig. 2 (b) is low-pass filtered to estimate velocity without short-period fluctuation (shown by dashed line in Fig.2 (b)). The Reynolds stress and SS flux without the influence of short-period fluctuation is estimated using regression line shown in Fig. 9 (dashed line in Fig. 2 (c), (d)). Because the short-period fluctuation is a slow fluctuation over a period of 30 to 60 min, the correlation is unaffected by the fluctuation. Fig. 2 (c), (d) show evidence that the short-period fluctuation increases peak value of Reynolds stress and SS flux by factor of more than two.

CONCLUSION

In this study, the vertical structure and the frequency characteristics of short-period fluctuation, and the force exciting it in the Tone River Estuary are investigated. An analysis of field data reveals that short-period fluctuation is barotropic and forced by offshore water level fluctuation. This may be due to two mechanisms: water level fluctuation of small amplitude excites longitudinal seiche by resonance, and dominant offshore water level fluctuation excites significant oscillation in the estuary. To ascertain the result, an analytical solution of forced oscillation with radiation and friction damping are derived. The frequency response functions estimated from the observation and those calculated from the theory shows good agreement up to the fourth harmonics of seiche. It revealed that friction is a dominant mechanism of damping when the period is short (say $T < 1$ hr), but as frequency increases, radiation becomes more noticeable.

In the Tone River Estuary, short-period fluctuation induces significant velocity fluctuation, which appears to increase peak value of bottom shear stress and resuspension rate by factor of more than two. Although it is not clear if similar fluctuation exists in other estuaries, this study indicates implies that the short-period fluctuation could significantly influence sediment dynamics in estuaries significantly.

ACKNOWLEDGEMENT

Authors appreciate the provision of the water level data measured at the HORS by the Port and Airport Research Institute.

REFERENCES

1. Allen, G.P., J.C. Salomon, P. Bassoullet, Y. Du Penhoat and C. De Grandpre: Effects of tides on mixing and suspended sediment transport in macrotidal estuaries, Sedimentological Geology, 26, pp.69-90, 1980.
2. Jay,D.A. and J.D. Musiak: Particle trapping in estuarine tidal flows, J. Geophys. Res., 99(C10), pp.20445-20461, 1994.
3. Postma, H.: Sediment transport and sedimentation in the estuarine environment, American Association of Advanced Sciences, 83, pp.158-179, 1967.
4. Shimizu, K., M. Irie and T. Ishikawa ; A field study on near-bottom turbulence and resuspension of fine sediment in the Tone River Estuary, Annual Journal of Hydraulic Engineering, JSCE, Vol.48, pp.769-774, 2004. (in Japanese)
5. Shimizu, K., T. Ishikawa and M. Irie ; A field study of near-bottom turbulence and resuspension of fine sediment in Tone River Estuary, pp.2137-2143. *In* Environmental Hydraulics and Sutainable Water Management, Lee & Lam (ed.), Taylor & Francis Group, London, U.K., 2005.
6. Ishikawa, T., T. Suzuki and X. Qian, ; Hydraulic study of the onset of hypoxia in the Tone River Estuary, J. Hydraul. Eng., ASCE, Vol.130, No.5, 2004.
7. Hino, M.; Spectral analysis, Asakura-Syoten, Tokyo, Japan, pp.86-88, 1977. (in Japanese)
8. Ulrych, T.D., T.N. Bishop; Maximum entropy spectral analysis and autoregressive decomposition, Rev. Geophys. and Space Phys., Vol.13, No.1, 1975.
9. Hayashi, N, H. Takahashi and M. Yamamoto; Observation of long period waves in outer sea, Proceedings of Coastal Engineering, JSCE, Vol.25, pp.14-17, 1978. (in Japanese)
10. Horikawa, K. ; Coastal Engineering - An introduction to Ocean Engineering, University of Tokyo Press, Tokyo, Japan, p.142, pp.159-160 & p.184 1978.
11. de Waele, Stijn and P.M.T. Broersen ; The Burg algorithm for segments, IEEE transactions on signal processing, Vol.48, No.10, pp.2876-2880, 2000.
12. Miles, J. and W. Munk ; Harbor paradox, J. Waterways and Harbor Division, Proceedings of ASCE, Vol.87, No.WW3, pp.111-130, 1961.
13. Ippen, A.T. and Y. Goda ; Wave induced oscillations in harbors: the solution for a rectangular harbor connected to the open-sea, Massachusetts Institute of Technology, Hydraulics Laboratory, Report No.59, 1963.

14. Goda, Y.; On secondary oscillation in rectangular and fan-shaped harbors – a solution using Fourier Transform, Proceedings of Annual Conference on Coastal Engineering, JSCE, Vol.10, pp.53-58, 1963. (in Japanese)
15. Unluata, U. and C.C. Mei ; Effects of entrance loss on harbor oscillation, J. Waterway, Harbor, Coastal Engineering Division, ASCE, Vol.101, No.WW2, pp.161-180, 1975.
16. Cerovecki, I., M. Orlic and M.C. Hendershott ; Adriatic seiche decay and energy loss to the Mediterranean, Deep Sea Res. I, Vol.44, No.12, pp.2007-2029, 1997.
17. Timoshenko,S., D.H. Young and W. Weaver, Jr. ; Vibration problems in engineering, John Wiley & Sons, New York, U.S.A., pp.72-88, 1974.
18. Ono, K. ; Engineering mechanics in the age of mechatoronics, Baifu-Kan Syoten, Tokyo, Japan, pp.176-180, 1999. (in Japanese)
19. Ikeda, S. ; Detailed Hydraulics, Gihodo-Syuppan, Tokyo, Japan, pp.249-250, 1999. (in Japanese)

APPENDIX – NOTATION

The following symbol are used in this paper:

a = constant given by Eq. 22;
b = width of river mouth;
c = phase velocity ;
C = suspended sediment concentration;
C_1, C_2 = constants of integration in Eq. 16;
f, f_e, f_r, f_s = water surface displacement function in general, in estuary, in sea, and that due to radiation from the mouth, respectively;
f_b = bottom friction coefficient;
F_r = Fourier transform of function f_r;
g = acceleration due to gravity;
h = mean water depth;
H_ζ, H_U = frequency response function of water level and velocity;
k, k_e, k_s = wave number in general, in estuary, and in sea;
k_{er}, k_{ei} = real and imaginary part of k_e;
k_{sy} = y component of k_s;

L = length of an estuary;

m = lag number used in Burg's method;

n = order of harmonics;

$n_{Manning}$ = Manning's roughness coefficient;

N = total number of data;

$P_U, P_\zeta, P_{\zeta_0}$ = Power spectrum of U, ζ, and ζ_0, respectively;

R = hydraulic radius;

S_1, S_2 = constant given by Eqs. 23 and 24;

t = time;

T, T_n = period in general and natural period;

u = velocity in x direction;

U, U_0 = depth averaged velocity in x direction in general and at the mouth;

V = depth averaged velocity in y direction;

w = vertical velocity;

x, x' = longitudinal coordinates taken as shown in Fig. 6;

y = transverse coordinate taken as shown in Fig. 6;

α = dummy variable in Eq. 18;

γ = linear dissipation coefficient;

$\varepsilon_{lin}, \varepsilon_{quad}$ = energy dissipated in an estuary over one period by linear and quadratic friction;

φ = constant given by Eq. 22;

ψ_1, ψ_2 = radiation functions defined by Eq. 18;

ω = angular frequency;

ξ = displacement of water parcel; and

ζ, ζ_0 = water surface displacement in general, and at the mouth.

(Received September 16, 2005 ; revised February 3, 2006)